Sensing with chirality pure near infrared fluorescent carbon nanotubes

Robert Nißler,[1] Larissa Kurth,[1] Han Li,[2] Alexander Spreinat,[1] Ilyas Kuhlemann,[1] Benjamin S. Flavel[2] and Sebastian Kruss[1,3,4*]

[1]Institute of Physical Chemistry, Göttingen University, Germany

[2]Institute of Nanotechnology, Karlsruhe Institute of Technology (KIT), Germany

[3]Department of Chemistry, Bochum University, Germany

[4]Fraunhofer Institute for Microelectronic Circuits and Systems

KEYWORDS: Biosensors, carbon nanotubes, chirality, near infrared fluorescence, multiplexing, dopamine

ABSTRACT: Semiconducting single wall carbon nanotubes (SWCNTs) fluoresce in the near infrared (NIR) and the emission wavelength depends on their chirality (*n*,*m*). Interactions with the environment affect the fluorescence and can be tailored by functionalizing SWCNTs with biopolymers such as DNA, which is the basis for fluorescent biosensors. So far, such biosensors were mainly assembled from mixtures of SWCNT chiralities with large spectral overlap, which affects sensitivity as well as selectivity and prevents multiplexed sensing. The main challenge to gain chirality pure sensors has been to combine approaches to isolate specific SWCNTs and generic (bio)functionalization approaches. Here, we created chirality pure SWCNT-based NIR biosensors for important analytes such as neurotransmitters and investigated the impact of SWCNT chirality/handedness as well as long-term stability and sensitivity. For this purpose, we used aqueous two-phase extraction (ATPE) to gain chirality pure (6,5)-, (7,5)-, (9,4)- and (7,6)-SWCNTs (emission at ~ 990, 1040, 1115 and 1130 nm). Exchange of the surfactant sodium deoxycholate (DOC) to specific single-stranded (ss)DNA sequences yielded monochiral sensors for small analytes (dopamine, riboflavin, ascorbic acid, pH). DOC used in the separation process was completely removed because residues impaired sensing. The assembled monochiral sensors were up to 10 times brighter than their non-purified counterparts and the ssDNA sequence affected absolute fluorescence intensity as well as colloidal (long-term) stability and selectivity for the analytes. $(GT)_{40}$-(6,5)-SWCNTs displayed the maximum fluorescence response to the neurotransmitter dopamine (+140 %, K_d = 1.9 x10^{-7} M) and a long-term stability > 14 days. Furthermore, the specific ssDNA sequences imparted selectivity to the analytes independent of SWCNT chirality and handedness of (+/-) (6,5)-SWCNTs. These monochiral/single-color SWCNTs enabled ratiometric/multiplexed sensing of dopamine, riboflavin, H_2O_2 and pH. In summary, we demonstrated the assembly, characteristics and potential of monochiral (single-color) SWCNTs for multiple NIR fluorescent sensing applications.

Introduction

Single wall carbon nanotubes (SWCNTs) are 1D nanomaterials with unique photophysical properties.[1–4] Semiconducting SWCNTs show fluorescence in the near infrared (NIR) region of the electromagnetic spectrum (optical tissue transparency window), which offers ultra-low background and high tissue penetration.[5] The emission wavelength depends on their chiral index/chirality (*n*,*m*)[6] and they are versatile building blocks for NIR labels and sensors.[7–11] As nanosensors they are powerful tools to study biological processes with high spatial, temporal and chemical resolution.[12–19] Most prominent examples are detection of signaling molecules such as neurotransmitters[12,20,21], reactive oxygen species (ROS)[13,14] or nitric oxide (NO)[17]. Additionally, sensing concepts have been developed for genetic material[15,22], lipids[23] or proteins[24–26]. Such sensors are not only able to report the presence of the molecule but imaging of many of them allows one to get spatiotemporal chemical information.[27] Using this concept for example release and secretion of the neurotransmitters dopamine and serotonin from cells could be resolved. [12,21] So far NIR fluorescent sensors based on SWCNTs have been assembled mainly from as-synthesized SWCNT material, which contains multiple chiralities, catalyst residues and impurities. However, for the simultaneous detection of different analytes, multiple sensors with unambiguous fluorescence emission and hence SWCNT chirality are required. Synthesis of chirality enriched SWCNTs improved over the last years, but commercially available SWCNT materials still contain multiple chiralites.[28,29] Therefore, separation and purification approaches are required to obtain samples with well-defined characteristics.[30,31] SWCNTs have been separated by centrifugation[32,33], gel chromatography[34–36], ion exchange chromatography[37] or aqueous two-phase extraction (ATPE)[38–40]. Furthermore, certain macromolecules such as single-stranded (ss)DNA sequences[41,42] or polyfluorenes (PFOs)[43] preferentially solubilize certain chiralities, which provides a route to monochiral samples. In the past years ATPE of SWCNTs made tremendous progress in isolation of various small and large SWCNT chiralities.[40,44–47] In this approach SWCNTs are dispersed either in a surfactant such as deoxycholate (DOC) or chirality-specific ssDNA[48,49] sequences and

separated between aqueous phases of two different polymers. This fast, reliable and low-cost separation method appears to be an optimal starting point to obtain monochiral sensors. Unfortunately, chirality pure SWCNTs obtained by these approaches are coated with the macromolecule or surfactant used for the purification process. The surfactant can be removed but the purer a sample becomes the more the hydrophobic SWCNTs tend to stick to each other and redispersion in other surfactants and biopolymers becomes difficult.[50]

In contrast, the chemical design of sensors requires functionalization with biomolecules that impart specificity to the SWCNT. Chemical approaches include non-covalent functionalization with DNA[42], peptides[51], peptide-DNA conjugates[52], protein-DNA conjugates[16,53], proteins[26] and lipids[24,54]. Recently, also sp^3 quantum defects on SWCNTs have been modified covalently with biomolecules.[55] Overall, the surface chemistry is crucial for molecular recognition and signal transduction. One of the best studied systems so far are DNA functionalized SWCNTs that recognize small molecules. Certain sequences make the SWCNT sensitive to biomolecules for example to the neurotransmitter dopamine[20,56]. In this particular case, it was shown that interactions of the two hydroxy groups of dopamine with the DNA backbone cause conformational changes that lead to an increase in quantum yield.[12,57] In contrast, simple adsorption and redox-chemistry could be ruled out.[57,58]

Consequently, the surface chemistry on SWCNTs is the most important part to tailor sensor properties but this has not been explored in detail and combined with purified monochiral SWCNTs. The above-mentioned difficulties impaired so far the obvious next step to use monochiral SWCNTs as building blocks for NIR fluorescent sensors and labels.

Here, we isolate monochiral SWCNTs to assemble single-color fluorescent sensors and study the impact of chirality and surface functionalisation on fluorescent sensing of biomolecules. For this purpose, we combine ATPE with exchange methods to various ssDNA sequences (including aptamers) and polymers. We quantify and compare the photophysical properties, stability and fluorescence responses of monochiral and multichiral sensors. Finally, we use the non-overlapping emission spectra of monochiral SWCNTs to demonstrate ratiometric and multiplexed sensing approaches.

Results and Discussion

To create nanosensors with narrow emission spectra chirality pure SWCNTs are necessary and we used a scalable ATPE approach that yields large amounts of exemplaric (6,5)-SWCNTs (Figure 1 a,b and Supplementary Figure S1). Exchange and variation of the ssDNA surface modification enabled the synthesis of different nanosensors, which were evaluated regarding their optical properties, colloidal stability and sensitivity in biosensing (Figure 1 c,d).

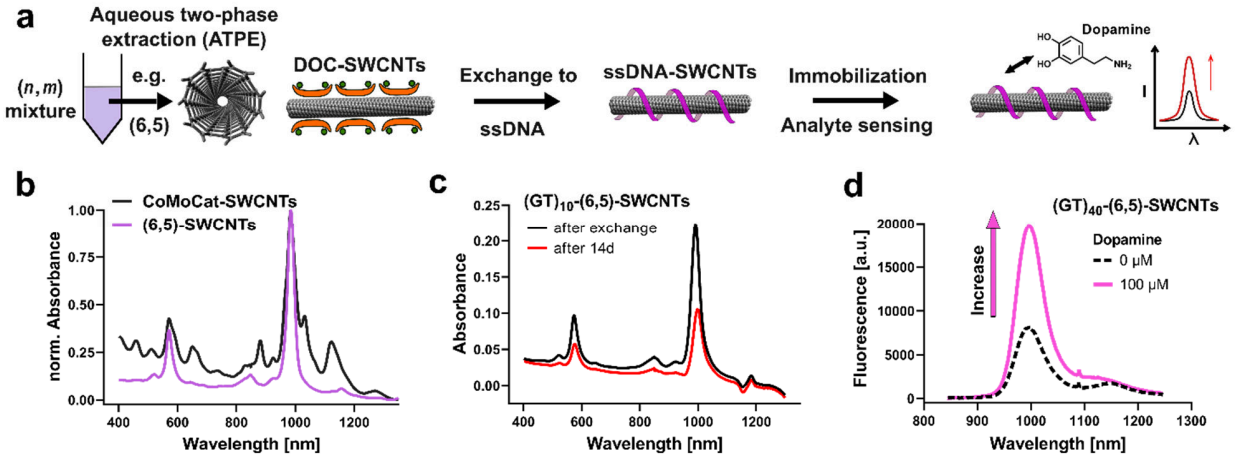

Figure 1 Assembly of chirality pure near infrared fluorescent carbon nanotube-based sensors. *a) Schematic of the workflow. Aqueous two-phase extraction (ATPE) yields chirality pure SWCNTs (e.g. (6,5)-SWCNTs) from a parental mixture. Exchange of the organic corona from the surfactant sodium deoxycholate (DOC) to single-stranded (ss)DNA or other (bio)polymers leads to monochiral functionalized SWCNTs that serve as sensors for small molecules such as the neurotransmitter dopamine. b) Exemplary normalized absorbance spectrum of parental CoMoCat-SWCNTs and purified (6,5)-SWCNTs in 1% DOC. c) Nine different ssDNA-(6,5)-SWCNTs were assessed. Here, exemplary absorbance spectra of $(GT)_{10}$-(6,5)-SWCNTs directly after surface exchange and after 14 days are shown. d) ssDNA-SWCNTs were immobilized on a glass surface and exposed to analytes that change their NIR fluorescence in a DNA sequence dependent way. Here, the exemplary monochiral fluorescence spectrum of a sensor for the neurotransmitter dopamine sensor is shown.*

Impact of ssDNA sequence on brightness and stability. Variation of the ssDNA sequence leads to ssDNA/SWCNT conjugates that are sensitive to different biologically important molecules.[56,59] Therefore, we first evaluated the influence of ssDNA sequence on the surface exchange process and optical properties. For this purpose, DOC-(6,5)-SWCNTs (Figure 1b) of the same concentration/absorbance (see Supplementary Figure S2) were exchanged to different ssDNA sequences. A typical

ssDNA-(6,5)-SWCNT absorption spectrum is shown in Figure 1c and the analysis of all E_{11} absorption features for the different ssDNA-(6,5)-SWCNTs after surface exchange is summarized in Figure 2a. All monochiral nanosensors displayed an absorbance maximum between 990.2 and 991.6 nm but large differences in absolute absorption. ssDNA sequences were able to redisperse 10 % (T_{30}) - 40 % ($(GT)_{40}$) of the parent surfactant stabilized (6,5)-SWCNTs in 1% DOC. When diluting all ssDNA-(6,5)-SWCNTs to an equal concentration[60] (0.2 nM in PBS), strong differences in fluorescence emission (Figure 2b) appeared. $(AT)_{15}$-SWCNTs showed both the strongest fluorescence emission as chirality pure as well as unpurified (CoMoCat)-SWCNTs (see Supplementary Figure S3 and S4). A different example is $(A)_{30}$-SWCNTs, which showed the lowest fluorescence intensity for non-purified CoMoCat-SWCNTs but high fluorescence emission for chirality pure (6,5)-SWCNTs. Distinct differences between chirality pure ssDNA-(6,5)-SWCNTs were also observed in terms of colloidal stability. We observed that some monochiral ssDNA-SWCNTs are less stable. This finding can be attributed to a higher purity without catalysts residues or amorphous carbon. Consequently, the hydrophobic interactions between SWCNTs could become stronger and increase aggregation tendencies. Measurements over 14 days revealed a decrease in E_{11} absorbance, as well as concomitant red shift for $(GT)_5$-(6,5)-SWCNTs. In contrast, $(GC)_{15}$-(6,5)-SWCNTs spectra remained stable (Figure 2c, Supplementary Figure S3 and S4). Both, decrease in absorbance and redshifting (broadening) are known parameters indicating SWCNT aggregation and hence loss of colloidal stability.[61] The analysis of all used ssDNA sequences (after 14 days) indicated that C_{30}- and $(GC)_{15}$-(6,5)-SWCNTs were most stable (Figure 2d), whereas $(GT)_5$- to $(GT)_{20}$-(6,5)-SWCNTs lost > 50% of the initial absorbance accompanied with a strong redshift (for more details see Supplementary Figure S5). In contrast, the longer $(GT)_{40}$ sequence showed a high colloidal stability. This result shows that ssDNA sequence and length play a crucial role for the properties of such monochiral conjugates.

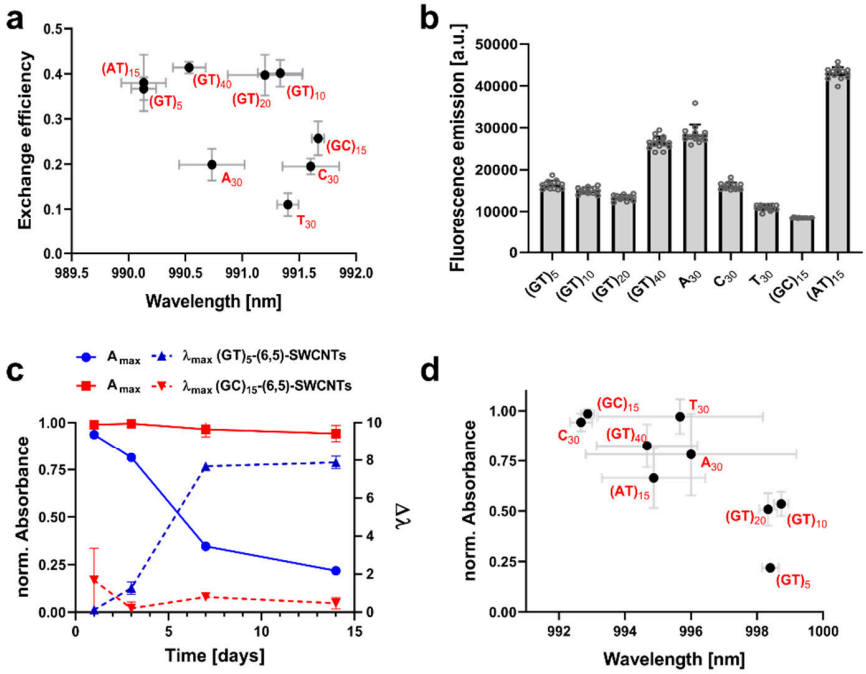

Figure 2: Surface exchange and colloidal stability of chirality pure ssDNA-(6,5)-SWCNTs. *a) Exchange efficiency and E_{11} absorbance maxima of nine different ssDNA-(6,5)-SWCNTs for surfactant exchanges to ssDNA (n=3, mean ± SE). All monochiral nanosensors have very similar absorbance features (maxima and fwhm of E_{11} transmission). b) Fluorescence intensities of 0.2 nM ssDNA-(6,5)-SWCNTs. $(AT)_{15}$-(6,5)-SWCNTs show the highest fluorescence emission (mean ± SD, n = 15, technical replicates from three independent exchange experiments). c) Normalized E_{11} absorbance and wavelength shift evaluated after 1, 3, 7 and 14 days post (6,5)-SWCNT surface exchange to ssDNA for two exemplary sequences. $(GT)_5$-(6,5)-SWCNTs show a decrease in absorbance and redshift, which indicates lower colloidal stability. In contrast, for example $(GC)_{15}$-(6,5)-SWCNTs remain stable over weeks (mean ± SE, n = 3). d) Colloidal stability for different ssDNA sequences as measured by the normalized E_{11} absorbance 14 days after surface exchange (mean ± SE, n = 3).*

Sensitivity of monochiral sensors. Chemical sensing with SWCNTs is a powerful tool to resolve biological processes in a spatiotemporal manner, even down to single-molecule interactions.[12,17,21,62] With distinct chirality pure and hence multi-color sensors, it would be possible to visualize and study multiple analytes simultaneously. To mimic this scenario and rule out possible colloidal stability effects, chemical sensing of the monochiral ssDNA-SWCNTs was performed after physisorption onto a glass surface. Analytes which are known to modulate the fluorescence intensity of unpurified SWCNTs in

solution were added.[57,58] A typical NIR fluorescence spectrum is shown in Figure 3a and 3b. Unpurified DNA-SWCNTs were challenged in the same way, to compare the chemical sensing behavior of monochiral and multichiral SWCNT sensors. The fluorescence responses for $(GT)_{40}$-(6,5)-SWCNTs are highlighted in Figure 3c and a summary for all nanosensors is presented in Figure 3d.

The overall responses showed the same trends for monochiral and multichiral ssDNA-(6,5)-SWCNTs, indicating that the sensing mechanism is preserved after SWCNT purification (see Supplementary Figure S6). The intensity of fluorescence response depended on the ssDNA sequence. In most cases, the response magnitude was stronger for non-purified DNA-SWNCTs e.g. after 10 µM dopamine addition +120 % for $(GT)_{40}$-(6,5)-SWCNTs and +250 % for parental $(GT)_{40}$-(CoMoCat)-SWCNTs. In some cases, such as T_{30}- and $(AT)_{15}$-(6,5)-SWCNTs (see Figure 3a and Supplementary Figure S6) the absolute sensor response was enhanced for monochiral sensors. The observed differences in analyte sensing responses (e.g. for dopamine sensing) are however not in correlation with the observed trend, that monochiral (6,5)-SWCNTs showed an up to 10x stronger fluorescence emission (see Supplementary Figure S7). Therefore, the higher brightness of monochiral SWCNTs does in general not come with the disadvantage of lower relative sensor responses.

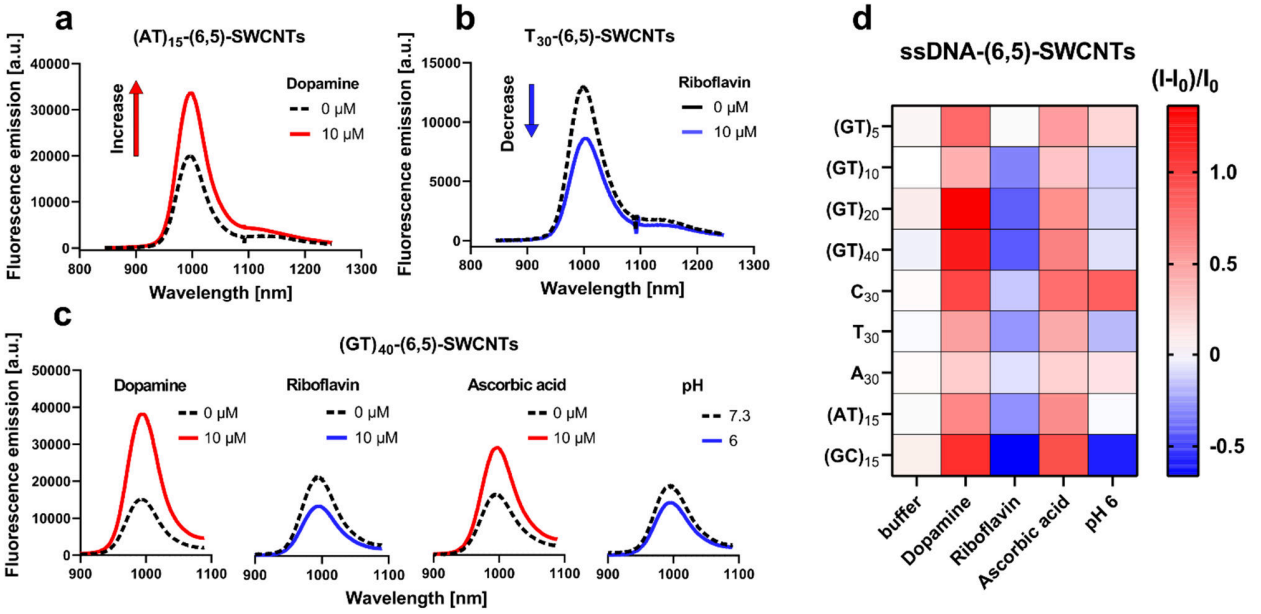

Figure 3: Sensitivity of monochiral ssDNA-(6,5)-SWCNT-based sensors. *Exemplary NIR fluorescence spectra: a) $(AT)_{15}$-(6,5)-SWCNTs increase their fluorescence in the presence of the neurotransmitter dopamine. b) T_{30}-(6,5)-SWCNTs decrease their fluorescence in the presence of riboflavin. c) Fluorescence response of $(GT)_{40}$-(6,5)-SWCNTs for different analytes. d) Overview of the responses of different functionalized (6,5)-SWCNTs. Fluorescence increases are shown in shades of red and fluorescence decreases in shades of blue (mean, n = 3). Dopamine, riboflavin and ascorbic acid concentration = 10 µM.*

As oligonucleotide length appeared to play an important role for chemical sensing with monochiral $(GT)_x$-(6,5)-SWCNTs, a dose-response curve for dopamine sensing was collected (Figure 4a and 4b). $(GT)_5$-(6,5)-SWCNTs increased by +40 % increase and saturated at ~1 µM dopamine with a dissociation constant K_d of 9.2 x10^{-8} M. A much stronger increase of intensity was observed for $(GT)_{40}$-(6,5)-SWCNTs (+140 %, saturation at ~10 µM, K_d = 1.9 x10^{-7} M). Furthermore, we evaluated how dopamine sensing is affected by DOC, which is a potential residue of the purification and surface exchange process. Addition of DOC ≥ 0.01 % (w/v) increased fluorescence of $(GT)_{40}$-(6,5)-SWCNTs (e.g. +500 % for 0.01 % DOC) and diminished the response to dopamine (Figure 4c). A similar trend was also observed when dopamine sensing was performed one hour after addition of DOC or when using $(GT)_5$-(6,5)-SWCNTs (Supplementary Figure S8). This result shows that in our exchange procedure no or negligible amounts of DOC are present in the system and the complete removal is necessary for non-biased chemical sensing with monochiral sensors.

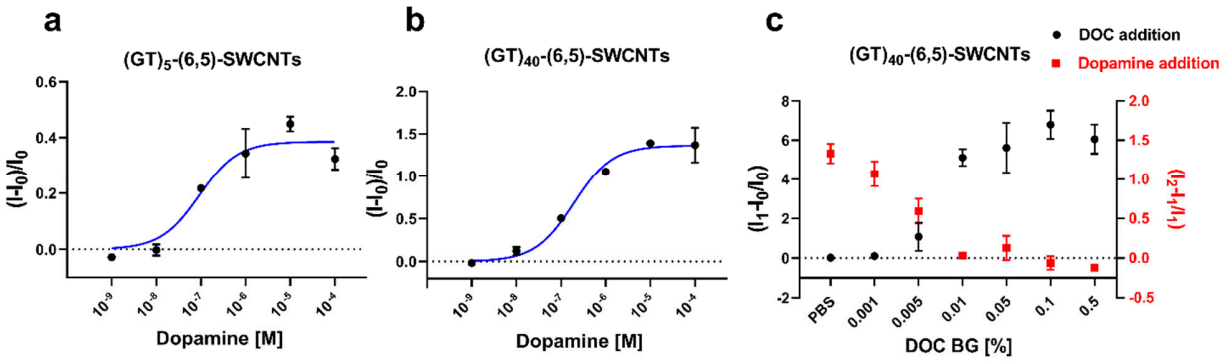

Figure 4: Sensitivity of $(GT)_x$-(6,5)-SWCNT dopamine sensors and impact of surfactant residues. *a) Dose dependent fluorescence response of $(GT)_5$-(6,5)-SWCNTs shows a maximum increase of ~ 40% and a K_d value of 9.2 x10^{-8} M Dopamine (mean ± SE, n = 3). Blue curve = fit. b) $(GT)_{40}$-(6,5)-SWCNTs show a maximum of ~ 140% fluorescence increase with a K_d value of 1.1 x10^{-7} M Dopamine (mean ± SE, n = 3). c) Dopamine sensing (10 µM) with DOC background. Addition of ≥ 0.01 % DOC (w/v) (black datapoints, I_1) to $(GT)_{40}$-(6,5)-SWCNTs abolishes fluorescent sensing (red datapoints, I_2) (mean ± SE, n = 3).*

Impact of SWCNT chirality and handedness. By using ATPE not only specific SWCNT chiralities but also SWCNT enantiomers can be isolated[40,44,45]. We wanted to find out if the handedness itself has an impact on sensing and calls for tailored functionalization. ssDNA modified enantiomers of (6,5)-SWCNTs can react differently to oxidizing agents.[48] For a further level of chiral interaction, stereoisomers of ascorbic acid and the catecholamine adrenaline were tested. We hypothesized that the response of sensors based on enantiomer pure SWCNTs might differ for the enantiomers of an analyte such as adrenaline. $(GT)_{40}$-ssDNA was used for surface modification, because of its beneficial features regarding exchange efficiency, colloidal stability and especially analyte sensing response.

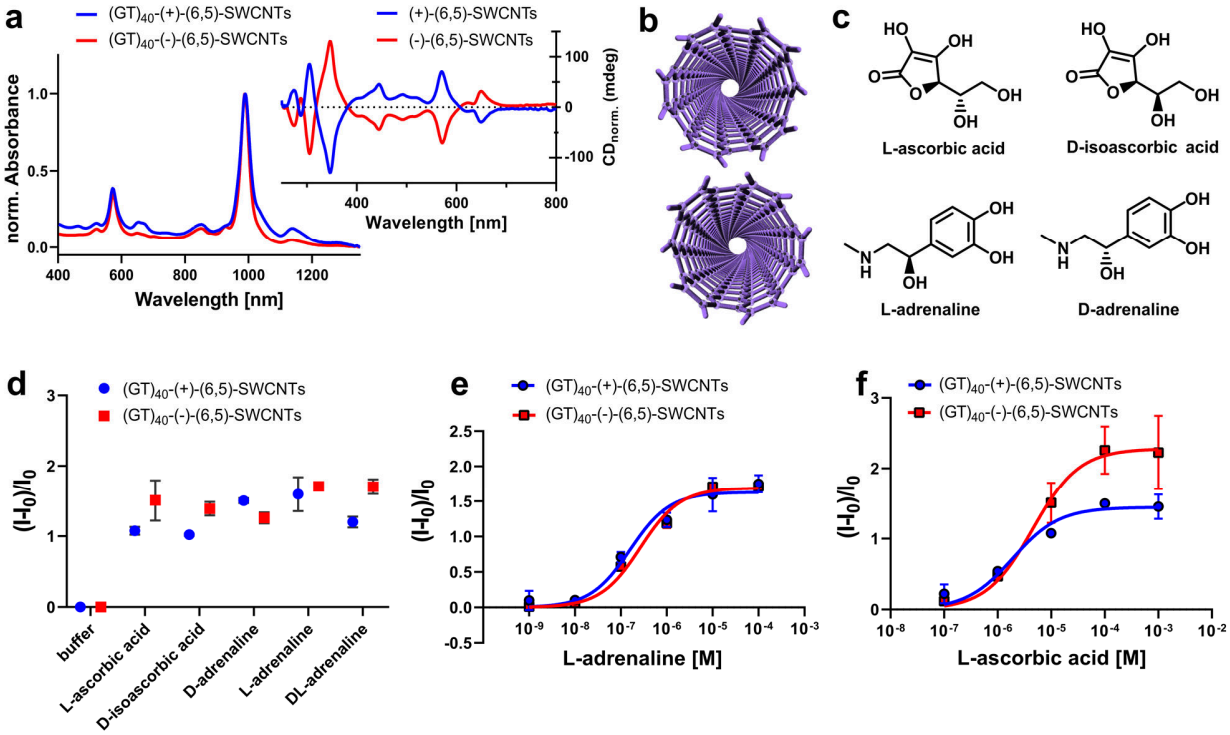

Figure 5: Sensing with (6,5)-SWCNT enantiomers. *a) Normalized absorbance spectra of (6,5)-SWCNT enantiomers with $(GT)_{40}$-ssDNA surface modification. The inset shows the CD spectra of both (6,5)-SWCNT enantiomers. b) Illustration of helical chirality of both (-)- and (+)-(6,5)-SWCNTs. c) Tested chiral molecules. d) Fluorescence response of $(GT)_{40}$-(+)-(6,5)-SWCNTs and $(GT)_{40}$-(-)-(6,5)-SWCNTs to stereoisomers of ascorbic acid and adrenaline (mean ± SD, n = 3, analytes = 10 µM). e) Dose-response curve of L-adrenaline and in f) for L-ascorbic acid using $(GT)_{40}$-(+)-(6,5)-SWCNTs and $(GT)_{40}$-(-)-(6,5)-SWCNTs (mean ± SD, n = 3, blue and red curves = fit).*

The enantiomer purity, based on the CD-spectra (Figure 5a) was calculated for both enantiomer fractions to be ~80 % (see Supplementary Figure S9).[63,64] Further surface exchange to $(GT)_{40}$ ssDNA yielded defined enantiomer-pure ssDNA-SWCNT conjugates, used for sensing experiments (Figure 5a and 5b). No significant differences between the stereoisomers were found, while $(GT)_{40}$-(-)-(6,5)-SWCNTs reacted with a stronger response to ascorbic acid, than $(GT)_{40}$-(+)-(6,5)-SWCNTs (Figure 5d) for ascorbic acid. To rule out that fluorescence changes after analyte addition (10 µM final concentration) are biased by a possible saturation, we collected dose-response curves. The results (Figure 5 e,f) indicate no difference in the response to stereoisomers of adrenalin but higher fluorescence responses for (-)-(6,5) enantiomer towards ascorbic acids (see also Supplementary Figure S10). Therefore, we conclude that the sensing and recognition mechanism is not significantly affected by the handedness of the SWCNT and the chirality of these analytes. Most likely, the diffusion of the exciton is affected mainly by the interaction between analyte and SWCNT and the chirality/bandgap energy plays a minor role for the fate of the exciton. As discussed already beforehand[48], the conformation and 3D structure of the surface adsorbed ssDNA could differ between the enantiomers and might be the reason for the differences in sensing magnitudes.

Multicolor and ratiometric sensing. ATPE is not only feasible for (6,5)-SWCNTs but also other chiralities, which opens the possibility to nanosensors with tunable emission wavelengths. To study the effect of the SWCNT chirality on sensing, we used ATPE-separated (7,5)-, (9,4)- and (7,6)-SWCNTs (see Supplementary Figure S11) and exchanged the surface modification again to ssDNA. This exchange process could be performed in a similar way as shown with (6,5)-SWCNTs, leading to monochiral $(GT)_{40}$-SWCNTs (Figure 6a). The distinct emission features of the used SWCNT chiralities (Figure 6b) highlight the potential for multi-color applications.

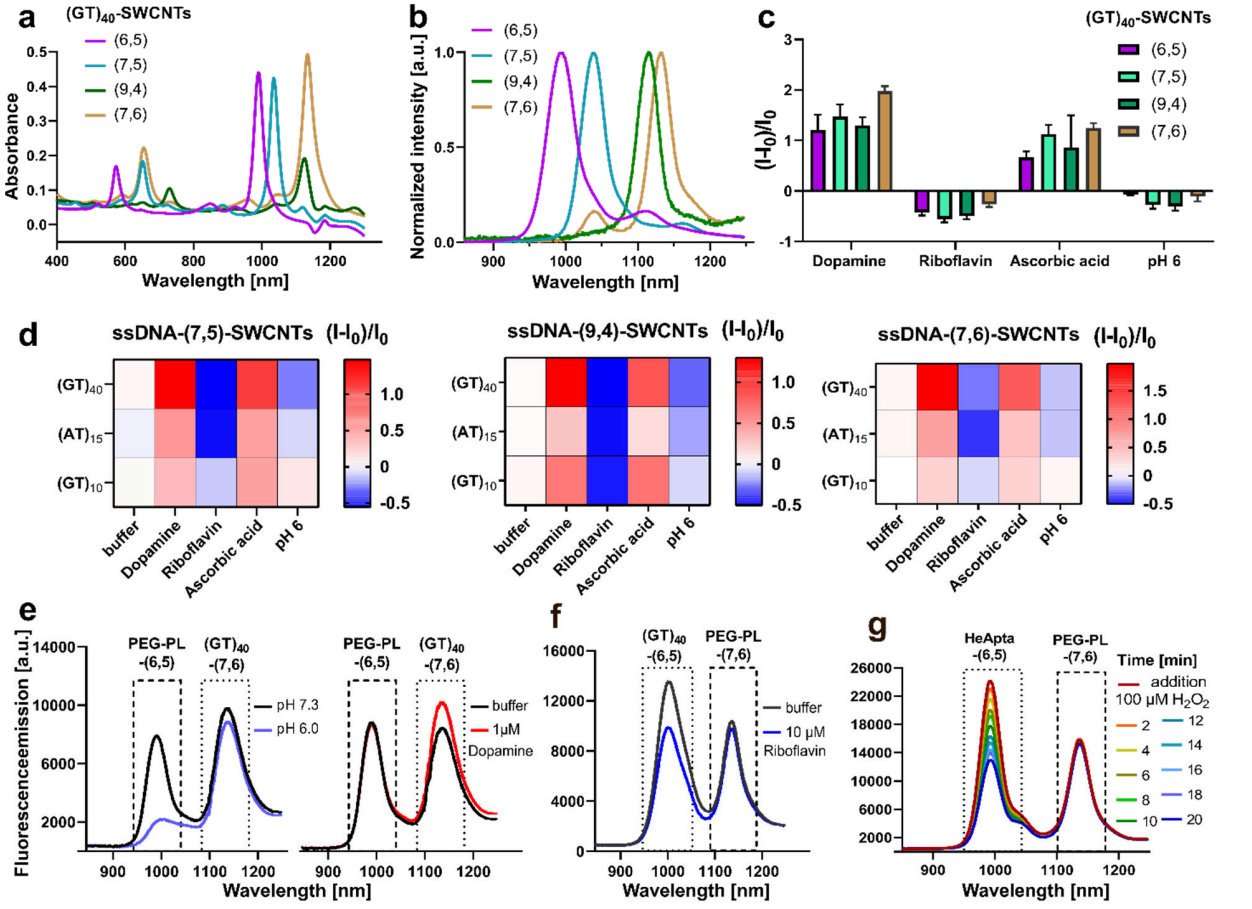

Figure 6: Multicolor and ratiometric sensing with monochiral SWCNTs. *a) Absorbance spectra of different monochiral $(GT)_{40}$-SWCNTs. b) Normalized fluorescence spectra, excited at the E_{22} transition (570 nm for (6,5)-SWCNTs, 650 nm for (7,5)-SWCNTs, 730 nm for (9,4)-SWCNTs, 650 nm for (7,6)-SWCNTs). c) Responses of monochiral $(GT)_{40}$-SWCNTs are similar for different chiralities (mean ± SD, n = 3, analytes = 10 µM). d) Fluorescence response of ssDNA-(7,5)-, ssDNA-(9,4)- and ssDNA-(7,6)-SWCNT nanosensors to different analytes (mean, n = 3, analytes = 10 µM). e) Ratiometric sensing of pH change (blue) and dopamine (red) using PEG-PL-(6,5)-SWCNTs and $(GT)_{40}$-(7,6)-SWCNTs. f) Ratiometric riboflavin sensing with $(GT)_{40}$-(6,5)-SWCNT and PEG-PL-(7,6)-SWCNTs as reference. g) Ratiometric H_2O_2 sensor with a hemin binding aptamer (HeApta)-(6,5)-SWCNTs and PEG-PL-(7,6)-SWCNTs as reference.*

Sensing (Figure 6c) experiments regarding the analytes dopamine, pH, riboflavin and ascorbic acid showed similar trends as monochiral (6,5)-SWCNTs (Figure 6d, Figure 3c and Supplement Fig. S12). We did not find a strong impact of SWCNT chirality on the sensor responses as reported in a few cases for non-purified SWCNT samples.[65] However, the results shown in Figure 6 are the first with monochiral SWCNTs for these analytes and with well-defined concentrations. Therefore, it is likely that SWCNT chirality plays a minor role for the sensors presented here. The combination of specifically modified monochiral sensors enabled furthermore ratiometric sensing (Figure 6e-g). Based on the variable nanosensor design (see Supplement Fig. S13 and Fig. S14) both, the (6,5)- and the (7,6)-SWCNTs can be either modified with ssDNA (e.g. responsive to riboflavine or dopamine) or with poly(ethylene glycol)-phospholipid (PEG-PL) as reference. Another ratiometric sensor detects H_2O_2 at µM concentrations (Figure 6g). Here, the SWCNT was modified with an aptamer that binds a protoporphyrin (hemin), which was shown to create an effective H_2O_2-sensor.[13] These results show that the design of SWCNT functionalization to receive sensors for specific analytes does not need to be changed for different chiralities of SWCNTs. For example, the 'reference' SWCNT in ratiometric sensing can be either (6,5) or (7,6) (Figure 6 e,f). Consequently, these chemical design concepts are universal and enable ratiometric sensors for multiple analytes.

Discussion

Chemical sensors are powerful tools to detect biomolecules and shed light on biological processes. Fluorescent nanosensors are able to report local properties and provide the high spatial and temporal resolution that is needed to study for example cellular communication in networks of cells or even *in vivo*[12,21,27]. Nevertheless, the biochemical complexity asks for detection of multiple analytes, which underlines the need for multiplexing approaches. Therefore, sensors/probes should have non-overlapping fluorescence spectra. SWCNT-based NIR fluorescent nanosensors have shown great potential to detect a range of biomolecules from neurotransmitters, reactive oxygen species, proteins, lipids and nucleic acids.[12,13,15,24] However, in most cases the samples contained multiple chiralities of SWCNTs, which leads to congested spectra and prevents multiplexing. Additionally, it is known that in solution the concentration of a SWCNT chirality affects sensor responsivity due to direct and photophysical chirality dependent interactions.[20,65,66] These processes lead to a bias in sensitivity and hampers selectivity. Additionally, it does not guarantee that the exact response measured in a mixed sample can be replicated in a single chirality sample. In this work we used SWCNT purification to get close to monochiral samples to create sensors and identify factors that affect sensitivity and selectivity. Until now only few studies[23,67], aimed to work with chirality pure sensors, but a general concept with tunable sensor design and emission wavelength is missing. This lack of progress can be explained by the experimental challenges to exchange the surface chemistry required for purification to the surface chemistry required for sensing.

To obtain single SWCNT chiralities different approaches have been developed and ATPE-based protocols recently showed great potential.[40,44,45] This technique does not require expensive equipment such as ultracentrifuges or chromatography-materials and yields SWCNTs dispersed in a surfactant in aqueous solution. However, even if the surface exchange of PFO-sorted SWCNTs was recently established *via* CPEP[50] (corona phase exchange purification), most SWCNT separation methods rely on aqueously dispersed SWCNTs. Such a SWCNT solution can be further exchanged by a variety of biopolymers. For this DOC-to-ssDNA exchange process[68], we used the commercially available PEG (6 kDa) as polymer, which we evaluated beforehand to do not effect further chemical sensing experiments. The maximum yield of redispersed SWCNTs by ssDNA with ~ 40 % was lower than originally described by Streit et al.[68] DNA strands can form different ordered structures on the same SWCNT chirality, which affect binding energies.[69,70] This could explain the influence of ssDNA sequence on SWCNT redispersion and colloidal stability over time.

Purified SWCNTs were brighter at the same concentration (based on the absorption at the E_{11} transition) compared to non-purified CoMoCat samples. This result was expected because the ATPE process most likely removes quenching impurities such as catalyst residues or metallic SWCNTs. For non-purified SWCNTs there is a tendency to observe the strongest fluorescence modulation for shorter $(GT)_x$ sequences.[56] In this context $(GT)_{10}$-ssDNA displayed the smallest dissociation constant (K_d) of 9.2 nM, which allows even to distinguish structurally closely related catecholamines.[56] For non-purified, high-pressure carbon monoxide (HiPco)-synthesized SWCNT samples $(GT)_{15}$-ssDNA showed a K_d value of 433 nM for (7,6)-SWCNTs.[20] Similarly, non-purified HiPco samples with $(GT)_6$-ssDNA for (9,4)-SWCNTs displayed K_d value of 10 µM.[71]

All these reported fluorescence changes and K_d value are solution measurements of mixed samples that could be biased by colloidal stability issues and complex interactions. For monochiral SWCNTs immobilized on a surface we found the strongest dopamine responses for $(GT)_{40}$-SWCNTs. Most other studies in literature used mixed chirality SWCNT sensors in solution. However, non-specific interactions or aggregation is minimized on a surface. The evaluated K_d value for $(GT)_{40}$-(6,5)-SWCNTs of 190 nM outlines the potential for neurotransmitter imaging in fast biological prosesses.[27]

Additionally, we studied to our knowledge for the first time enantiomer-pure ssDNA-SWCNTs for sensing. No significant difference was observed for the chiral catecholamine adrenalin, indicating that analyte sensing and recognition mechanism is not affected by the stereochemical conformation of the small molecules. On the other hand the absolute differences in response by (-)- and (+)-(6,5)-SWCNTs with $(GT)_{40}$-ssDNAsurface modification were slightly different (sensing of ascorbic acids). They could be attributed to small differences in the DNA conformation on the enantiomers of one SWCNT chirality. Those variations were shown to be relevant for differences in oxidation potential to NaOCl.[48] Recent studies furthermore confirmed possible DNA-structure differences between SWCNT enantiomers[72] and also between sonicated and surface-exchanged ssDNA-SWNCTs[73].

Our results indicate that the handedness of the SWCNT does not change the sensing mechanism at least for these catecholamine sensors. The current understanding is that the interaction between the catechol moiety and the phosphate backbone leads to conformational changes that affect exciton dynamics.[12]

Consequently, the chiral part of the catecholamines plays a less important role. Based on these results enantiomers of one chirality are not changing or reducing sensor performance. However, it does not rule out that for other sensing mechanisms the handedness of the SWCNT itself plays a role.

Sensing with (7,5)-, (9,4)-, and (7,6)-SWCNTs showed qualitatively very similar results as for ssDNA-(6,5)-SWCNTs, e.g. 120 – 190 % fluorescence increase for $(GT)_{40}$-SWCNTs after dopamine addition. It is known that the fluorescence response to analytes can be influenced by the SWCNT sensor concentration and therefore we performed these experiments with exactly the same SWCNT concentration.[66] These experiments are the first ones outside of mixtures and report fluorescence changes in a well-defined system.

The developed approach to exchange the coating DOC of chirality pure SWCNTs to a biopolymer is feasible for all kinds of chirality pure samples (Figure 6). From this large-scale and stable stock solutions , various sensors can be created by methanol-based exchange[68], which opens the possibilities to all desirable combinations of SWCNT chiralities (emission features) and diverse surface modifications (sensing and recognitions units). Technical and conceptual challenges have so far prevented the preparation of tunable monochiral sensors. In our work we show the potential and difficulties such as surfactant residues (Figure 3) in the preparation of monochiral SWCNT-based sensors. The shown ratiometric and multiplexed sensing techniques will enhance the robustness as well as sensitivity of imaging approaches for example to resolve neurotransmitter release.[12,21] Furthermore, it is likely that selectivity and cross-reactivity can be improved. Additionally, our characterization of sensors made from homogenous nanomaterials provides a much clearer picture on the impact of heterogeneity of nanomaterials on their function.

Conclusion

In summary, we systematically studied the properties of monochiral ssDNA-SWCNT NIR fluorescent sensors. We developed a robust surface functionalization exchange process and show how ssDNA sequence and length affects colloidal stability, photophysics and sensing. It allowed us to gain insights into the impact of chirality, handedness and residues from SWCNT separation on sensitivity of sensors for multiple analytes. Consequently, NIR ratiometric sensors for the important analytes dopamine, riboflavin and H_2O_2 or pH changes could be demonstrated. These conceptual and mechanistic insights pave the way for tailored multi-color and ratiometric biosensing and imaging applications.

Materials and Methods

All materials, if not otherwise stated, were purchased from Sigma Aldrich.

SWCNT surface modification

(6,5)-chirality enriched CoMoCat SWCNTs (Sigma-Aldrich, product no. 773735) were modified with varying single-stranded (ss)DNA such as $(GT)_5$, $(GT)_{10}$, $(GT)_{20}$, $(GT)_{40}$, $(C)_{30}$, $(A)_{30}$, $(T)_{30}$, $(GC)_{15}$, $(GA)_{15}$ and $(AT)_{15}$ (oligonucleotide sequences purchased by Sigma Aldrich) followed a previously described protocol.[58] Hereby, 100 µL ssDNA (2 mg/mL in H_2O) were mixed with 100 µL 2xPBS and 100 µL SWCNTs (2 mg/mL in PBS), tip-sonicated for 15 min @ 30% amplitude (36 W output power, Fisher Scientific model 120 Sonic Dismembrator) and centrifuged 2x 30 min @ 16100x g. DOC-dispersed SWCNTs were obtained by tip-sonicating 4 mg CoMoCat SWCNTs in 2 ml 1% DOC for 30 min @ 40% amplitude, followed by 2x 30 min centrifugation @ 16100x g.

SWCNT separation

Separation of (6,5)-SWCNTs was performed according to a previously reported aqueous two-phase extraction (ATPE) protocol from Li *et al*.[40] Briefly, in a three step approach SWCNT chiralities were separated between two aqueous phases, containing dextran (MW 70000 Da, 4% m/m) and PEG (MW 6000 Da, 8% m/m) with varying pH-values *via* HCl addition. The final B3 (bottom)-phase yielded monochiral (6,5)-SWCNTs which were diluted with DOC to obtain a stable 1% DOC-SWCNT solution. Dialysis (300 kDa dialysis bag, Spectra/Por®, Spectrum Laboratories Inc.) against 1% DOC removed the dextran polymer, used for SWCNT separation. The separation of (7,5)- and (9,4)-SWCNTs was following the similar pH-modulated ATPE process as described above. Instead of 0.05% DOC and 0.5% SDS for normal process, 0.07% DOC and 0.5% SDS was used here to improve the resolution of (7,5)- as well as (9,4)-SWCNTs. Enantiomer pure (6,5)-SWCNTs were prepared by increasing SDS carefully with a fixed DOC concentration. Similar diameter sorting based on DOC/SDS was performed first with a constant 0.04% DOC and a increasing SDS content from 0.5 to 1.25% in order to remove all species larger than (6,5)-SWCNTs. Then SDS concentrations were increased very slowly and step by step from 1.3%, 1.35%, 1.4% to 1.45% (T14, T15, T16 and T17). All of these four continuous fractions (T14 – T17) are (6,5) enriched. After the further semiconducting-metallic separation, T14 and T16 with an obvious shift (3 nm) at E_{11} transition were selected for further experiments. (7,6)-SWCNTs was obtained by using the similar ATPE method but from a different CoMoCAT raw soot (CHASM, lot#: SG76-L39). Briefly a 3-stage ATPE process was used to sort single chirality (7,6). In Stage-1, SDS concentrations were changed from 0.5% to 1.5% with a constant DOC concentration (0.04%) to get a (7,6)-enriched top fraction (T4, with SDS ~ 0.7%). Then fresh bottom phase was added to T4 and SDS concentrations were again changed from 0.6% to 1% with the same DOC 0.04% to further purify this enriched (7,6) fraction. In the end, a metal-semi separation was performed to remove the metallic tubes at Stage-3.

Enantiomer (6,5)-SWCNTs were prepared by a similar diameter sorting based on DOC/SDS.[38] First the concentrations of SDS 0.9% and DOC 0.04% were used in order to push all species larger than (6,5)-SWCNTs to the top phase and remove them. Then SDS concentrations were increased very slowly and step by step to 1.3%. The next seven continuous fractions (T1 – T7) were collected and all of them are (6,5) enriched. After the next semiconducting-metallic separation, T2 was found to be highly enantiomer (-)-(6,5) enriched. Sodium cholate (SC) was then used to further separate highly enriched (+)-(6,5) from the fraction T4 CD measurements were performed on an CD spectrometer (J-1500, JASCO) from 800 nm to 200 nm through a 1 mm path length cuvette in 1 nm steps (scanning speed 100 nm/min, bandwidth ~2.2 nm).

Monochiral SWCNT surface exchange towards ssDNA

Surface exchange of the SWCNTs towards ssDNA was achieved by applying the steps from Streit *et al*.[68] Purified (6,5)-SWCNTs in 1% DOC were diluted to an absorbance of 2.0 at the E_{11} transition (986 nm). Concentration of (7,5)-SWCNTS was 2.0 at 1032 nm, for (9,4)-SWNCTs 0.9 at 1112 nm and for (7,6)-SWCNTs 1.6 at 1129 nm. 150 µl of purified SWCNTs in 1% DOC were mixed with 25 µl of PEG (MW 6 kDa, 25% m/v) and 30 µl of ssDNA (2.0 mg/mL in H_2O). After one precipitation cycle, due to stepwise addition of 270 µL methanol and subsequent addition of 600 µL isopropyl alcohol, the loose nanotube pellet was separated from the supernatant by short (1s) centrifugation @ 16100x g. The supernatant was further centrifuged for 2 min @ 16100x g, and the obtained residue DNA pellet was redispersed in 300 µL 1xPBS. This solution was used to redisperse the nanotube pellet by bath sonication or 10 sec tip-sonication. Further centrifugation (5 min @ 16100x g) yielded the monochiral nanosensors, which were characterized afterwards by absorption spectroscopy. For stability measurements the ssDNA-(6,5)-SWCNTs were diluted to an absorbance at the E_{11} transition (~991 nm) of 0.2 and measured again after time intervals of 1, 3, 7 and 14 days. Surface exchange towards PEG-PL (18:0 PEG5000 PE, Avanti Lipids) was performed following a modified protocol.[54] DOC-dispersed chirality pure SWCNT fractions were concentrated and washed with sodium cholate (SC, 12 mg/ml in PBS) using molecular cut-off spin filtration (Vivaspin 500, 100000 Da molecular weight cut-off, Sartorius). 800 µl of these SC-SWCNTs were mixed with 2 mg 18:0 PEG5000 PE dissolved in 200 µL PBS and dialyzed 2 days against 1xPBS, using a 1 kDa cut-off dialysis tube. The final PEG-PL-SWCNTs were obtained after 20 min of centrifugation @ 16100x g. For ratiometric H_2O_2 sensing, the hemin-binding aptamer (HeApta) 5′- AGT GTG AAA TAT CTA AAC TAA ATG TGG AGG GTG GGA CGG GAA GAA GTT TAT TTT TCA CAC T-3′ was used[13,74], with a concentration of 50 nM hemin.

NIR spectroscopy

Absorption spectra were acquired with a JASCO V-670 device from 400 to 1350 nm in 0.2 nm steps in a 10 mm path glass-cuvette. 1D-NIR fluorescence spectra were measured with a Shamrock 193i spectrometer (Andor Technology Ltd., Belfast, Northern Ireland) connected to a IX53 Microscope (Olympus, Tokyo, Japan). Excitation was performed with a gem 561 laser (Laser Quantum, Stockport, UK). 2D excitation emission spectra were collected with a Monochromator MSH150, equipped with a LSE341 light source (LOT-Quantum Design GmbH, Darmstadt, Germany) as excitation source.

NIR fluorescence analyte response measurements were performed, by letting 60 µl of a 0.2 nM ssDNA-SWCNT solution (concentration calculation based on previous literature[60,75,76]) adsorb overnight (12 h) on a glass bottom 96-well plate (#1 cover glass, 0.13-0.16 mm, Cellvis, P96-1-N), followed by washing with PBS and addition of 20 µl analyte to 180 µl buffer solution (PBS). Fluorescence spectra were acquired with 130 mW excitation @561 nm and 10 sec integration time. D-adrenaline was purchased from AKos GmbH (Lörrach, Germany). Dose-response measurements were fitted with a one site – specific binding fit (GraphPad Prism 8) using Y = Bmax * X / (K_d + X) with X = concentration of the analyte; Y = specific binding; Bmax = Maximum binding and K_d = dissociation constant.

ASSOCIATED CONTENT

Supporting Information. S1: Aqueous two-phase extraction (ATPE)-based isolation of (6,5)-SWCNTs. S2: (6,5)-SWCNTs in 1% DOC. S3: Baseline corrected ssDNA-SWCNT absorbance spectra for colloidal stability evaluation. S4: Colloidal stability and spectral shifts of ssDNA-CoMoCat-SWCNTs. S5: Time dependent colloidal stability of ssDNA-SWCNTs. S6: Chemical sensing with surface immobilized multichiral ssDNA-(CoMoCat)-SWCNTs. S7: Comparison of the fluorescence intensity of monochiral and multichiral ssDNA-SWCNTs. S8: Dopamine sensing in the presence of surfactant (DOC) background. S9: Properties of (6,5)-SWCNT enantiomers. S10: Sensing with ssDNA-(6,5)-SWCNT enantiomers. S11: Separation of (7,5)-, (9,4)- and (7,6)-SWCNTs. S12: Chemical sensing with single chirality ssDNA-SWCNTs. S13: Nanosensor surface design for ratiometric sensing. S14: Monochiral and ratiometric analyte sensing.

AUTHOR INFORMATION

Corresponding Author

* skruss@uni-goettingen.de

Author Contributions

R.N. and S.K. designed and conceived the research S.K. coordinated the project. L.K. and R.N. separated (6,5)-SWCNTs, performed and characterized surface exchange and chemical sensing experiments, A.S. and I.K. wrote python-based analysis scripts for absorbance and sensing evaluation, H.L. and B.F. separated (7,5)-, (9,4)- and (7,6)-SWCNTs and enantiomers of (6,5)-SWCNTs. All authors contributed to the writing of the manuscript and analysis of data.

Funding Sources

Volkswagen Foundation, Deutsche Forschungsgemeinschaft (DFG)

Notes

There are no competing financial interests.

ACKNOWLEDGMENT

This project was supported by the VW foundation and the DFG.

ABBREVIATIONS

SWCNT, single walled carbon nanotubes; ATPE, aqueous two-phase extraction; DOC, sodium deoxycholate; ssDNA, single stranded deoxyribonucleic acid; PEG-PL poly(ethylenglycol)-phospholipid

REFERENCES

(1) Li, J.; Pandey, G. P. Advanced Physical Chemistry of Carbon Nanotubes. *Annu. Rev. Phys. Chem.* **2015**, *66* (1), 331–356.

(2) Zamolo, V. Z.; Vazquez, E.; Prato, M. Carbon Nanotubes: Synthesis, Structure, Functionalization, and Characterization. *Top. Curr. Chem.* **2013**, *286* (March), 1–72.

(3) Nanot, S.; Hároz, E. H.; Kim, J. H.; Hauge, R. H.; Kono, J. Optoelectronic Properties of Single-Wall Carbon Nanotubes. *Adv. Mater.* **2012**, *24* (36), 4977–4994.

(4) Amori, A. R.; Hou, Z.; Krauss, T. D. Excitons in Single-Walled Carbon Nanotubes and Their Dynamics. *Annu. Rev. Phys. Chem.* **2018**, *69* (1), 81–100.

(5) O'Connell, M. J.; Bachilo, S. M.; Huffman, C. B.; Moore, V. C.;

Strano, M. S.; Haroz, E. H.; Rialon, K. L.; Boul, P. J.; Noon, W. H.; Kittrell, C.; et al. Band Gap Fluorescence from Individual Single-Walled Carbon Nanotubes. *Science (80-.).* **2002**, *297* (5581), 593–596.

(6) Bachilo, S. M.; Strano, M. S.; Kittrell, C.; Hauge, R. H.; Smalley, R. E.; Weisman, R. B. Structure-Assigned Optical Spectra of Single-Walled Carbon Nanotubes. *Science (80-.).* **2002**, *298* (December), 2361–2367.

(7) Kruss, S.; Hilmer, A. J.; Zhang, J.; Reuel, N. F.; Mu, B.; Strano, M. S. Carbon Nanotubes as Optical Biomedical Sensors. *Adv. Drug Deliv. Rev.* **2013**, *65* (15), 1933–1950.

(8) Hong, G.; Diao, S.; Antaris, A. L.; Dai, H. Carbon Nanomaterials for Biological Imaging and Nanomedicinal Therapy. *Chem. Rev.* **2015**, *115* (19), 10816–10906.

(9) Farrera, C.; Torres Andón, F.; Feliu, N. Carbon Nanotubes as Optical Sensors in Biomedicine. *ACS Nano* **2017**, *11* (11), 10637–10643.

(10) Hendler-Neumark, A.; Bisker, G. Fluorescent Single-Walled Carbon Nanotubes for Protein Detection. *Sensors (Switzerland)* **2019**, *19* (24).

(11) Dinarvand, M.; Elizarova, S.; Daniel, J.; Kruss, S. Imaging of Monoamine Neurotransmitters with Fluorescent Nanoscale Sensors. *Chempluschem* **2020**, *85* (7), 1465–1480.

(12) Kruss, S.; Salem, D. P.; Vuković, L.; Lima, B.; Vander Ende, E.; Boyden, E. S.; Strano, M. S. High-Resolution Imaging of Cellular Dopamine Efflux Using a Fluorescent Nanosensor Array. *Proc. Natl. Acad. Sci.* **2017**, *114* (8), 1789–1794.

(13) Wu, H.; Nißler, R.; Morris, V.; Herrmann, N.; Hu, P.; Jeon, S.; Kruss, S.; Giraldo, J. P. Monitoring Plant Health with Near-Infrared Fluorescent H2O2 Nanosensors. *Nano Lett.* **2020**, *20* (4), 2432–2442.

(14) Lew, T. T. S.; Koman, V. B.; Silmore, K. S.; Seo, J. S.; Gordiichuk, P.; Kwak, S.-Y.; Park, M.; Ang, M. C.-Y.; Khong, D. T.; Lee, M. A.; et al. Real-Time Detection of Wound-Induced H2O2 Signalling Waves in Plants with Optical Nanosensors. *Nat. Plants* **2020**, *6* (4), 404–415.

(15) Harvey, J. D.; Jena, P. V.; Baker, H. A.; Zerze, G. H.; Williams, R. M.; Galassi, T. V.; Roxbury, D.; Mittal, J.; Heller, D. A. A Carbon Nanotube Reporter of MicroRNA Hybridization Events in Vivo. *Nat. Biomed. Eng.* **2017**, *1* (4), 1–43.

(16) Williams, R. M.; Lee, C.; Galassi, T. V.; Harvey, J. D.; Leicher, R.; Sirenko, M.; Dorso, M. A.; Shah, J.; Olvera, N.; Dao, F.; et al. Noninvasive Ovarian Cancer Biomarker Detection via an Optical Nanosensor Implant. *Sci. Adv.* **2018**, *4* (4).

(17) Kim, J. H.; Heller, D. A.; Jin, H.; Barone, P. W.; Song, C.; Zhang, J.; Trudel, L. J.; Wogan, G. N.; Tannenbaum, S. R.; Strano, M. S. The Rational Design of Nitric Oxide Selectivity in Single-Walled Carbon Nanotube near-Infrared Fluorescence Sensors for Biological Detection. *Nat. Chem.* **2009**, *1* (6), 473–481.

(18) Gravely, M.; Safaee, M. M.; Roxbury, D. Biomolecular Functionalization of a Nanomaterial To Control Stability and Retention within Live Cells. *Nano Lett.* **2019**, *19* (9), 6203–6212.

(19) Beyene, A. G.; Delevich, K.; Del Bonis-O'Donnell, J. T.; Piekarski, D. J.; Lin, W. C.; Thomas, A. W.; Yang, S. J.; Kosillo, P.; Yang, D.; Prounis, G. S.; et al. Imaging Striatal Dopamine Release Using a Nongenetically Encoded near Infrared Fluorescent Catecholamine Nanosensor. *Sci. Adv.* **2019**, *5* (7), eaaw3108.

(20) Kruss, S.; Landry, M. P.; Vander Ende, E.; Lima, B. M. A.; Reuel, N. F.; Zhang, J.; Nelson, J.; Mu, B.; Hilmer, A.; Strano, M. Neurotransmitter Detection Using Corona Phase Molecular Recognition on Fluorescent Single-Walled Carbon Nanotube Sensors. *J. Am. Chem. Soc.* **2014**, *136* (2), 713–724.

(21) Dinarvand, M.; Neubert, E.; Meyer, D.; Selvaggio, G.; Mann, F. A.; Erpenbeck, L.; Kruss, S. Near-Infrared Imaging of Serotonin Release from Cells with Fluorescent Nanosensors. *Nano Lett.* **2019**, *19* (9), 6604–6611.

(22) Harvey, J. D.; Baker, H. A.; Ortiz, M. V.; Kentsis, A.; Heller, D. A. HIV Detection via a Carbon Nanotube RNA Sensor. *ACS Sensors* **2019**, *4* (5), 1236–1244.

(23) Galassi, T. V.; Jena, P. V.; Shah, J.; Ao, G.; Molitor, E.; Bram, Y.; Frankel, A.; Park, J.; Jessurun, J.; Ory, D. S.; et al. An Optical Nanoreporter of Endolysosomal Lipid Accumulation Reveals Enduring Effects of Diet on Hepatic Macrophages in Vivo. *Sci. Transl. Med.* **2018**, *10* (461), 1–11.

(24) Bisker, G.; Dong, J.; Park, H. D.; Iverson, N. M.; Ahn, J.; Nelson, J. T.; Landry, M. P.; Kruss, S.; Strano, M. S. Protein-Targeted Corona Phase Molecular Recognition. *Nat. Commun.* **2016**, *7*, 1–14.

(25) Bisker, G.; Bakh, N. A.; Lee, M. A.; Ahn, J.; Park, M.; O'Connell, E. B.; Iverson, N. M.; Strano, M. S. Insulin Detection Using a Corona Phase Molecular Recognition Site on Single-Walled Carbon Nanotubes. *ACS Sensors* **2018**, *3* (2), 367–377.

(26) Zubkovs, V.; Schuergers, N.; Lambert, B.; Ahunbay, E.; Boghossian, A. A. Mediatorless, Reversible Optical Nanosensor Enabled through Enzymatic Pocket Doping. *Small* **2017**, *13* (42), 1701654.

(27) Meyer, D.; Hagemann, A.; Kruss, S. Kinetic Requirements for Spatiotemporal Chemical Imaging with Fluorescent Nanosensors. *ACS Nano* **2017**, *11* (4), 4017–4027.

(28) Wang, J.-Q.; Ding, F.; Luo, D.; Zhang, D.; Wang, X.; Yang, J.; Bai, X.; Peng, F.; Xu, Z.; Wei, J.; et al. Chirality-Specific Growth of Single-Walled Carbon Nanotubes on Solid Alloy Catalysts. *Nature* **2014**, *510* (7506), 522–524.

(29) An, H.; Kumamoto, A.; Takezaki, H.; Ohyama, S.; Qian, Y.; Inoue, T.; Ikuhara, Y.; Chiashi, S.; Xiang, R.; Maruyama, S. Chirality Specific and Spatially Uniform Synthesis of Single-Walled Carbon Nanotubes from a Sputtered Co-W Bimetallic Catalyst. *Nanoscale* **2016**, *8* (30), 14523–14529.

(30) Yang, F.; Wang, M.; Zhang, D.; Yang, J.; Zheng, M.; Li, Y. Chirality Pure Carbon Nanotubes: Growth, Sorting, and Characterization. *Chem. Rev.* **2020**, *120* (5), 2693–2758.

(31) Zheng, M. Sorting Carbon Nanotubes. *Top. Curr. Chem.* **2017**, *375* (1), 1–36.

(32) Arnold, M. S.; Green, A. A.; Hulvat, J. F.; Stupp, S. I.; Hersam, M. C. Sorting Carbon Nanotubes by Electronic Structure Using Density Differentiation. *Nat. Nanotechnol.* **2006**, *1* (1), 60–65.

(33) Ghosh, S.; Bachilo, S. M.; Weisman, R. B. Advanced Sorting of Single-Walled Carbon Nanotubes by Nonlinear Density-Gradient Ultracentrifugation. *Nat. Nanotechnol.* **2010**, *5* (6), 443–450.

(34) Liu, H.; Nishide, D.; Tanaka, T.; Kataura, H. Large-Scale Single-Chirality Separation of Single-Wall Carbon Nanotubes by Simple Gel Chromatography. *Nat. Commun.* **2011**, *2*, 1–8.

(35) Flavel, B. S.; Kappes, M. M.; Krupke, R.; Hennrich, F. Separation of Single-Walled Carbon. **2013**, No. 4, 3557–3564.

(36) Tvrdy, K.; Jain, R. M.; Han, R.; Hilmer, A. J.; Mcnicholas, T. P.; Strano, M. S. A Kinetic Model for the Deterministic Prediction of Gel-Based Carbon Nanotube Separation. *ACS Nano* **2013**, *2*, 1779–1789.

(37) Tu, X.; Manohar, S.; Jagota, A.; Zheng, M. DNA Sequence Motifs for Structure-Specific Recognition and Separation of Carbon Nanotubes. *Nature* **2009**, *460* (7252), 250–253.

(38) Fagan, J. A.; Khripin, C. Y.; Silvera Batista, C. A.; Simpson, J. R.; Hároz, E. H.; Hight Walker, A. R.; Zheng, M. Isolation of Specific Small-Diameter Single-Wall Carbon Nanotube Species via Aqueous Two-Phase Extraction. *Adv. Mater.* **2014**, *26* (18), 2800–2804.

(39) Khripin, C. Y.; Fagan, J. A.; Zheng, M. Spontaneous Partition of Carbon Nanotubes in Polymer-Modified Aqueous Phases. *J. Am. Chem. Soc.* **2013**, *135* (18), 6822–6825.

(40) Li, H.; Gordeev, G.; Garrity, O.; Reich, S.; Flavel, B. S. Separation of Small-Diameter Single-Walled Carbon Nanotubes in One to Three Steps with Aqueous Two-Phase Extraction. *ACS Nano* **2019**, *13*, 2567–2578.

(41) Zheng, M.; Jagota, A.; Strano, M. S.; Santos, A. P.; Barone, P.; Chou, S. G.; Diner, B. A.; Dresselhaus, M. S.; Mclean, R. S.; Onoa, G. B.; et al. Structure-Based Carbon Nanotube Sorting by Sequence-Dependent DNA Assembly. *Science (80-.).* **2003**, *302*, 1545–1549.

(42) Zheng, M.; Jagota, A.; Semke, E. D.; Diner, B. A.; McLean, R. S.; Lustig, S. R.; Richardson, R. E.; Tassi, N. G. DNA-Assisted Dispersion and Separation of Carbon Nanotubes. *Nat. Mater.* **2003**, *2* (5), 338–342.

(43) Nish, A.; Hwang, J. Y.; Doig, J.; Nicholas, R. J. Highly Selective Dispersion of Single-Walled Carbon Nanotubes Using Aromatic Polymers. *Nat. Nanotechnol.* **2007**, *2* (10), 640–646.

(44) Fagan, J. A. Aqueous Two-Polymer Phase Extraction of Single-Wall Carbon Nanotubes Using Surfactants. *Nanoscale Adv.* **2019**, *1* (9), 3307–3324.
(45) Li, H.; Gordeev, G.; Garrity, O.; Peyyety, N. A.; Selvasundaram, P. B.; Dehm, S.; Krupke, R.; Cambré, S.; Wenseleers, W.; Reich, S.; et al. Separation of Specific Single-Enantiomer Single-Wall Carbon Nanotubes in the Large-Diameter Regime. *ACS Nano* **2020**, *14* (1), 948–963.
(46) Wei, L.; Flavel, B. S.; Li, W.; Krupke, R.; Chen, Y. Exploring the Upper Limit of Single-Walled Carbon Nanotube Purity by Multiple-Cycle Aqueous Two-Phase Separation. *Nanoscale* **2017**, *9* (32), 11640–11646.
(47) Sims, C. M.; Fagan, J. A. Near-Infrared Fluorescence as a Method for Determining Single-Wall Carbon Nanotube Extraction Conditions in Aqueous Two Polymer Phase Extraction. *Carbon N. Y.* **2020**, *165*, 196–203.
(48) Ao, G.; Streit, J. K.; Fagan, J. A.; Zheng, M. Differentiating Left- and Right-Handed Carbon Nanotubes by DNA. *J. Am. Chem. Soc.* **2016**, *138* (51), 16677–16685.
(49) Lyu, M.; Meany, B.; Yang, J.; Li, Y.; Zheng, M. Toward Complete Resolution of DNA/Carbon Nanotube Hybrids by Aqueous Two-Phase Systems. *J. Am. Chem. Soc.* **2019**, *141* (51), 20177–20186.
(50) Nißler, R.; Mann, F. A.; Preiß, H.; Selvaggio, G.; Herrmann, N.; Kruss, S. Chirality Enriched Carbon Nanotubes with Tunable Wrapping via Corona Phase Exchange Purification (CPEP). *Nanoscale* **2019**, *11* (23), 11159–11166.
(51) Mann, A. F.; Horlebein, J.; Meyer, N. F.; Thomas, F.; Kruss, S. Carbon Nanotubes Encapsulated in Coiled-Coil Peptide Barrels. *Chem. - A Eur. J.* **2018**, *24*, 12241–12245.
(52) Polo, E.; Nitka, T.; Neubert, E.; Erpenbeck, L.; Vuković, L.; Kruss. Control of Integrin Affinity by Confining RGD Peptides on Fluorescent Carbon Nanotubes. *ACS Appl. Mater. Interfaces* **2018**, *10*, 17693−17703.
(53) Mann, F. A.; Lv, Z.; Grosshans, J.; Opazo, F.; Kruss, S. Nanobody Conjugated Nanotubes for Targeted Near-Infrared in Vivo Imaging and Sensing. *Angew. Chemie Int. Ed.* **2019**, *58*, 1469–11473.
(54) Welsher, K.; Liu, Z.; Sherlock, S. P.; Robinson, J. T.; Chen, Z.; Daranciang, D.; Dai, H. A Route to Brightly Fluorescent Carbon Nanotubes for Near-Infrared Imaging in Mice. *Nat. Nanotechnol.* **2009**, *4* (11), 773–780.
(55) Mann, F. A.; Herrmann, N.; Opazo, F.; Kruss, S. Quantum Defects as a Toolbox for the Covalent Functionalization of Carbon Nanotubes with Peptides and Proteins. *Angew. Chemie - Int. Ed.* **2020**, 2–9.
(56) Mann, F. A.; Herrmann, N.; Meyer, D.; Kruss, S. Tuning Selectivity of Fluorescent Carbon Nanotube-Based Neurotransmitter Sensors. *Sensors* **2017**, *17*, 1521.
(57) Polo, E.; Kruss, S. Impact of Redox-Active Molecules on the Fluorescence of Polymer-Wrapped Carbon Nanotubes. *J. Phys. Chem. C* **2016**, *120* (5).
(58) Nißler, R.; Mann, F. A.; Chaturvedi, P.; Horlebein, J.; Meyer, D.; Vukovic, L.; Kruss, S. Quantification of the Number of Adsorbed DNA Molecules on Single-Walled Carbon Nanotubes. *J. Phys. Chem. C* **2019**, *123*, 4837–4847.
(59) Zhang, J.; Landry, M. P.; Barone, P. W.; Kim, J. H.; Lin, S.; Ulissi, Z. W.; Lin, D.; Mu, B.; Boghossian, A. A.; Hilmer, A. J.; et al. Molecular Recognition Using Corona Phase Complexes Made of Synthetic Polymers Adsorbed on Carbon Nanotubes. *Nat. Nanotechnol.* **2013**, *8* (12), 959–968.
(60) Schöppler, F.; Mann, C.; Hain, T. C.; Neubauer, F. M.; Privitera, G.; Bonaccorso, F.; Chu, D.; Ferrari, A. C.; Hertel, T. Molar Extinction Coefficient of Single-Wall Carbon Nanotubes. *J. Phys. Chem. C* **2011**, *115* (30), 14682–14686.
(61) O'Connell, M.; Bachilo, S.; Huffman, C.; Moore, V.; M., S.; E., H.; K., R.; P., B.; W., N.; C., K.; et al. Band Gap Fluorescence from Individual SWCNTs. *Science (80-.).* **2002**, *297* (July), 593–596.
(62) Meyer, D.; Telele, S.; Zelená, A.; Gillen, A. J.; Antonucci, A.; Neubert, E.; Nißler, R.; Mann, F. A.; Erpenbeck, L.; Boghossian, A. A.; et al. Transport and Programmed Release of Nanoscale Cargo from Cells by Using NETosis. *Nanoscale* **2020**, *12*, 9104–9115.
(63) Sato, N.; Tatsumi, Y.; Saito, R. Circular Dichroism of Single-Wall Carbon Nanotubes. *Phys. Rev. B* **2017**, *95* (15), 1–11.
(64) Wei, X.; Tanaka, T.; Hirakawa, T.; Yomogida, Y.; Kataura, H. Determination of Enantiomeric Purity of Single-Wall Carbon Nanotubes Using Flavin Mononucleotide. *J. Am. Chem. Soc.* **2017**, *139* (45), 16068–16071.
(65) Salem, D. P.; Landry, M. P.; Bisker, G.; Ahn, J.; Kruss, S.; Strano, M. S. Chirality Dependent Corona Phase Molecular Recognition of DNA-Wrapped Carbon Nanotubes. *Carbon N. Y.* **2016**, *97*.
(66) Landry, M. P.; Vukovic, L.; Kruss, S.; Bisker, G.; Landry, A. M.; Islam, S.; Jain, R.; Schulten, K.; Strano, M. S. Comparative Dynamics and Sequence Dependence of DNA and RNA Binding to Single Walled Carbon Nanotubes. *J. Phys. Chem. C* **2015**, No. 119, 10048−10058.
(67) Giraldo, J. P.; Landry, M. P.; Kwak, S. Y.; Jain, R. M.; Wong, M. H.; Iverson, N. M.; Ben-Naim, M.; Strano, M. S. A Ratiometric Sensor Using Single Chirality Near-Infrared Fluorescent Carbon Nanotubes: Application to in Vivo Monitoring. *Small* **2015**, *11* (32), 3973–3984.
(68) Streit, J. K.; Fagan, A.; Zheng, M. A Low Energy Route to DNA-Wrapped Carbon Nanotubes via Replacement of Bile Salt Surfactants. *Anal. Chem.* **2017**, *89*, 10496–10503.
(69) Roxbury, D.; Jagota, A.; Mittal, J. Structural Characteristics of Oligomeric DNA Strands Adsorbed onto Single-Walled Carbon Nanotubes. *J. Phys. Chem. B* **2013**, *117*, 132−140.
(70) Shankar, A.; Mittal, J.; Jagota, A. Binding between DNA and Carbon Nanotubes Strongly Depends upon Sequence and Chirality. *Langmuir* **2014**, *30* (11), 3176–3183.
(71) Beyene, A. G.; Alizadehmojarad, A. A.; Dorlhiac, G.; Goh, N.; Streets, A. M.; Král, P.; Vuković, L.; Landry, M. P. Ultralarge Modulation of Fluorescence by Neuromodulators in Carbon Nanotubes Functionalized with Self-Assembled Oligonucleotide Rings. *Nano Lett.* **2018**, *18* (11), 6995–7003.
(72) Zheng, Y.; Alizadehmojarad, A. A.; Bachilo, S. M.; Kolomeisky, A. B.; Weisman, R. B. Dye Quenching of Carbon Nanotube Fluorescence Reveals Structure-Selective Coating Coverage Dye Quenching of Carbon Nanotube Fluorescence Reveals Structure-. *ACS Nano* **2020**.
(73) Yang, Y.; Sharma, A.; Noetinger, G.; Zheng, M.; Jagota, A. Pathway-Dependent Structures of DNA-Wrapped Carbon Nanotubes: Direct Sonication vs Surfactant/DNA Exchange. *J. Phys. Chem. C* **2020**, *124* (16), 9045–9055.
(74) Pan, J.; Zhang, H.; Cha, T.-G. G.; Chen, H.; Choi, J. H.; Cha, T.-G. G.; Zhang, H.; Pan, J.; Chen, H. Multiplexed Optical Detection of Plasma Porphyrins Using DNA Aptamer-Functionalized Carbon Nanotubes. *Anal. Chem.* **2013**, *85* (17), 8391–8396.
(75) Streit, J. K.; Bachilo, S. M.; Ghosh, S.; Lin, C.; Weisman, R. B. Directly Measured Optical Absorption Cross Sections for Structure- Selected Single-Walled Carbon Nanotubes. *Nano Lett.* **2014**.
(76) Sanchez, S. R.; Bachilo, S. M.; Kadria-Vili, Y.; Lin, C. W.; Weisman, R. B. (N,m)-Specific Absorption Cross Sections of Single-Walled Carbon Nanotubes Measured by Variance Spectroscopy. *Nano Lett.* **2016**, *16* (11), 6903–6909.